TPM Vol. 32, No. S6, 2025
ISSN: 1972-6325
https://www.tpmap.org/

STUDY OF THE DESIGN OF AN H-SHAPED HYDRAULIC ENERGY DISSIPATOR BY CFD SIMULATIONS AND EXPERIMENTAL TESTS

VENTOCILLA ORTIZ MARIA FERNANDA
[1]CIVIL ENGINEERING UNDERGRADUATE STUDENT, UNIVERSIDAD PRIVADA DEL NORTE, FACULTY OF ENGINEERING, LIMA, PERU
EMAIL: n00322669@upn.pe, ORCID ID: HTTPS://ORCID.ORG/0009-0005-1746-2919

CAVERO TAMAYO JOSE MANUEL
CIVIL ENGINEERING UNDERGRADUATE STUDENT, UNIVERSIDAD PRIVADA DEL NORTE, FACULTY OF ENGINEERING, LIMA, PERU
EMAIL: n00338787@upn.pe, ORCID ID: HTTPS://ORCID.ORG/0009-0005-2347-000X

CARMONA ARTEAGA ABEL
MASTER OF SCIENCE IN WATER RESOURCES, UNIVERSIDAD PRIVADA DEL NORTE, FACULTY OF ENGINEERING, LIMA, PERU
EMAIL: abel.carmona@upn.edu.pe, ORCID ID: HTTPS://ORCID.ORG/0000-0003-2895-9582

Abstract— The main objective of this research was to evaluate the effectiveness of an "H" shaped energy dissipator design in reducing the velocity and controlling the flow of water in areas vulnerable to overflows, using both Autodesk CFD simulations and experimental tests. The performance of these dissipators was analyzed to optimize their dissipation capacity, analyzing factors such as block geometry, water flow pattern, and design configurations. Two-dimensional simulations and experimental data showed the behavior of the dissipators with the chosen shape under varying flow conditions, including water velocities and pressures. The results provided a better understanding of the interaction between water flow and energy dissipators, providing a basis for evaluating their impact in real-world scenarios. This research was based on theoretical and experimental principles of fluid mechanics, contributing to the application of dissipators to mitigate the effects of water overflows due to river flooding.
Keywords: Autodesk CFD, H-shaped blocks, hydraulic dissipation, loss of energy, vorticity.

INTRODUCTION

Peru is a country characterized by its geographic and climatic diversity, factors that, while it is true that they enrich its territory, also expose it to natural phenomena that put the population at risk. One of the biggest problems that has increased in recent decades is the overflow of rivers, a phenomenon that mainly affects rural and urban areas near river basins.

During periods of torrential rains, rivers increase not only their flow, but also their speed of flow, which increases the kinetic energy of the water. This phenomenon becomes a trigger for the erosion of the banks and flooding in vulnerable areas, affecting both the infrastructure and the safety of the people who live in the surrounding areas. Many of these disasters are aggravated by the unplanned occupation of the banks, where the inhabitants do not have the necessary resources to relocate to safer areas.

Faced with this problem, civil engineering and fluid mechanics play an important role in mitigating these disasters by designing infrastructures that can control or at least reduce the impacts of river floods. In this context, energy dissipators have emerged as a key solution. These systems can reduce the speed of water and dissipate its energy, minimizing the damage caused [1]. The design of dissipators, however, is not a simple task. It requires a deep analysis of the characteristics of the water flow, as well as simulations under different conditions that may occur.

Unfortunately, the study of fluid kinematics has always been complex, since its study requires solving highly difficult differential equations, which lack analytical solutions. This is evident in the Navier-Stokes equations, used to model fluid behavior [2]. The development of new technologies in recent years has allowed the creation of advanced software that facilitates the development of advanced software that facilitates the resolution and analysis of fluid behavior.

Recent research has shown that two-dimensional simulations performed using CFD are useful for studying phenomena such as energy dissipation.

I. RESEARCH OBJECTIVE

In response to the challenges posed, this research focuses on evaluating the effectiveness of "H" shaped hydraulic energy dissipators in reducing the velocity and pressure in the water flow. Through simulations in CFD software and experimental validations, the aim is to determine the influence of the created design as a hydraulic energy dissipator and evaluate its performance under realistic flow conditions, considering parameters such as Reynolds number, pressures, and velocity variations.

II. THEORETICAL FRAMEWORK

A. Autodesk Inventor

It is computer-aided design (CAD) software that allows you to create three-dimensional models with great precision. It presents a wide variety of advanced tools to perform correct modeling, optimizing the designs and then performing simulations [3].

B. Autodesk CFD

Digital simulation tool designed to model fluid behavior, providing accurate and efficient results. This software enables the analysis of key variables such as velocity, pressure, and turbulence, facilitating the prediction of fluid behavior under real-world conditions. It also offers graphical visualization of flow using streamlines, vectors, and color-coded contours. Furthermore, it allows the generation of simulation reports that provide detailed quantitative information. [4].

C. Reynolds number

The Reynolds number is defined as an essential dimensionless magnitude in fluid mechanics, which allows to characterize the flow regime that occurs inside a conduit or around an object. This number is defined as the relationship between the inertial forces and the viscous forces present in the fluid. In this way, obtaining this value allows classifying the flow as laminar or turbulent [5].

$$\mathrm{Re} = \frac{D \cdot v \cdot \rho}{\mu} \quad (1)$$

$$D_P = \frac{4 \cdot a \cdot b}{2(a+b)} \quad (2)$$

Re: Reynolds number
D: Hydraulic Diameter (m)
V: Fluid velocity (m/s)
ρ: Fluid density (kg/m^3)
μ: fluid dynamic viscosity (Pa.s)

D. Energy dissipator

Hydraulic energy dissipators are structures designed to reduce the speed and energy of water flow, preventing erosion, dissipating kinetic energy to prevent damage, and protecting nearby infrastructure. These devices allow the flow to decrease its energy through mechanisms such as hydraulic jumps, turbulence, or physical elements that divert the flow [6].

E. Laminar and turbulent flow

In fluid mechanics, flow can be classified as laminar and turbulent according to the Reynolds number (RE), especially in channels. Laminar flow (Re ≤ 500) is an ordered motion in parallel layers, where viscous forces dominate, forming a stable and uniform velocity profile. In contrast, turbulent flow (Re ≥ 500) is chaotic and irregular, characterized by intense interactions between particles and fluid layers due to the predominance of inertial forces [7].

F. Wakes

Wakes are described as patterns that form behind an object when a fluid flows around it. In hydraulic terms, the formation of a wake occurs when a solid object interrupts the flow, generating a low-pressure zone behind the figure. This phenomenon is marked by the appearance of eddies and turbulence, as the fluid moves irregularly to occupy the space left behind [8].

G. Drag Force

These are the resistances that a fluid exerts on an object as it moves through its environment. The magnitude of the drag force depends on the size, shape, and speed of the object, as well as the properties of the fluid, such as viscosity and density. Reducing this force is essential to improving flow efficiency.[9].

$$C_d = \frac{2 \cdot F \cdot d}{\rho \cdot v^2 \cdot A} \quad (3)$$

Cd: drag coefficient
ρ: fluid density
v: velocity of the free flow of the fluid relative to the body.
A: characteristic area of the body

H. Stagnation point

It is the location on the surface of an object where the fluid velocity is zero due to direct opposition to the flow. This point, which is located at the front of the object in an incident flow, marks the area of greatest pressure in the object's surroundings, as the kinetic energy of the fluid is completely converted into static pressure [10].

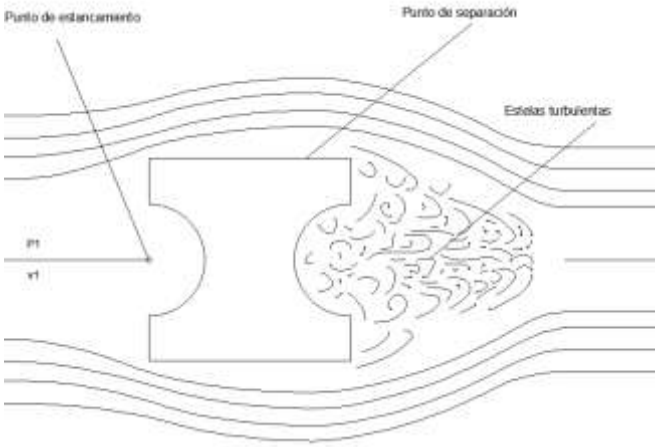

Fig. 1 Stagnation point of an H-shaped block in a fluid stream

I. Stagnation point

The stagnation point is defined as the place where the velocity within a flow field is equal to zero, this is due to the impact of the fluid with a surface or where the fluid will rest, in this way it can be concluded that it is also the place where there is the greatest pressure [10].

J. Shedding point

The shedding point is the place on the surface of an object where the laminar flow separates from the surface and enters a turbulent regime. From this point on, the fluid does not follow the shape of the object, generating a low-pressure region and a wake with vortices. The location of the shedding point depends on factors such as the Reynolds number and the geometry of the object [11].

K. Von Kárman effect

This effect refers to an oscillating pattern of vortices that forms in the wake of an object when it interrupts a fluid flow. These vortices are altered from one side to the other, creating a series of eddies. The frequency of these vortices is related to the Reynolds number and to better appreciate this effect their number must be greater than 1000 although it does not necessarily have to be a turbulent flow [12].

L. Vortices

These are flow regions where the flow particles rotate around a central axis, generating circular or spiral patterns. Vortices are common in turbulent flows and are indicative of energy loss and wake formation [13].

M. Sst Omega DES

This is a hybrid model used in the simulation of turbulent flows within the field of computational fluid dynamics (CFD). This model combines two turbulence simulation approaches: Reynolds-Averaged Navier-Stokes (RANS) and Large Eddy Simulation (LES). Both models are applied depending on the flow region and the characteristics of the turbulence [14].

N. Streamlines and tracelines

These lines are representations of the path of particles in a flow. Streamlines show the instantaneous direction of flow and help to identify high and low velocity zones at each point. In contrast, tracelines reflect the path of a particle over time, using tracers such as ink to visualize phenomena such as turbulence or vortex formation [15].

O. General energy equation

The energy equation is a fundamental expression in fluid mechanics that describes the conservation of energy in a flow system. This equation states that in a lossless flow, the sum of kinetic, potential, and pressure energies remains constant along a stream path. It is essential in the analysis of hydraulic systems and in the calculation of velocity, height, and pressure variations within a flow [16].

$$\frac{v_1^2}{2g} + \frac{P_1}{\gamma} + z_1 = \frac{v_2^2}{2g} + \frac{P_2}{\gamma} + z_2 + h_T \qquad (4)$$

v_1: Input speed (m/s)
v_2: Output speed (m/s)
P_1: Inlet pressure (Pa)
P_2: Outlet pressure (Pa)
Z_1: Elevation at first section

Z_2: Elevation at second section
g: Gravity (m/s²)
γ: Specific weight (N/m³)
h_T: Total losses

P. Geometrical and kinematic similarity

Kinematic similarity describes the patterns of fluid motion between similar systems and is directly related to geometric similarity. If two systems exhibit geometric similarity, with proportionally scaled dimensions, their flow patterns are expected to follow a kinematic pattern, if the flow conditions are the same. This allows the models to be studied at a reduced scale and results in being extrapolated to larger systems [17].

Q. Navier - Stokes equation

The Navier-Stokes equations are essential in fluid mechanics to model and understand the behavior of fluids under various conditions. We can say that these equations include both partial and ordinary differential equations so that they allow the analysis of variables such as speed and pressure, which change as a function of the independent variables. With the Navier-Stokes equation, it is achieved that, for incompressible fluids, the density of a fluid remains constant. [18]

$$\rho\frac{D_u}{D_t} = \left(-\frac{\partial P}{\partial x}\right) + (\rho \cdot g_x) + (\mu \cdot \nabla^2 \cdot u) \quad (5)$$

$$\rho\frac{D_v}{D_t} = \left(-\frac{\partial P}{\partial y}\right) + (\rho \cdot g_y) + (\mu \cdot \nabla^2 \cdot v) \quad (6)$$

$$\rho\frac{D_w}{D_t} = \left(-\frac{\partial P}{\partial z}\right) + (\rho \cdot g_z) + (\mu \cdot \nabla^2 \cdot w) \quad (7)$$

$$\nabla^2 = \frac{\partial^2}{\partial x^2} + \frac{\partial^2}{\partial y^2} + \frac{\partial^2}{\partial z^2} \quad (8)$$

∇^2: Nabla operator
ρ: Density
μ: Fluid viscosity
u,v,w: Velocity components in x, y and z directions

METHOD

The development and analysis of the flow in a simulation carried out in the Autodesk CFD program will allow us to evaluate how the H-shaped hydraulic energy dissipator behaves under different flow conditions, laminar and turbulent, considering the speeds. Therefore, it is important to carry out an adequate design that follows symmetry parameters and other criteria that optimize the performance of the dissipators.

To create the H-shaped figure, an energy dissipator model was designed that includes curves on the sides to generate wakes in the water flow. As can be seen in Figure 2 with its respective measurements. This effect contributes to the dissipation of energy by inducing abrupt changes in the direction and speed of the flow, thus increasing local turbulence and favoring the loss of kinetic energy.

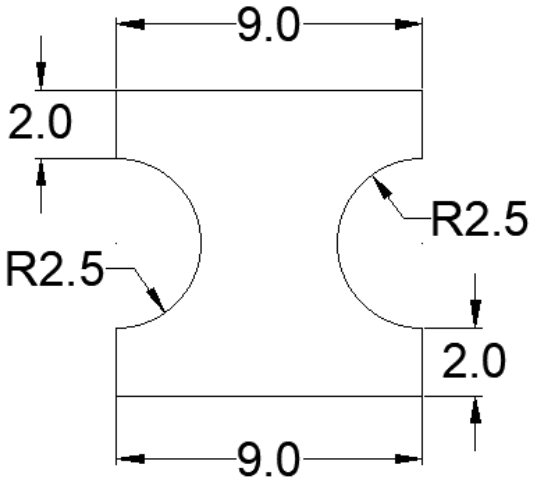

Fig. 2 Heatsink dimensions and design

The model was designed with dimensions of 9 x 9 cm and a curvature radius of 2.5 cm on each side to generate interaction between the flow, aiming to induce specific patterns of turbulence and energy dissipation.
This design was captured in AutoCAD, considering the dimensions of the flow table of the hydraulics laboratory of

the Universidad Privada del Norte. A vertical separation of 3.375 cm was established between each block, ensuring adequate spacing for flow interaction and reducing potential blockages. In addition, the horizontal distance between figures was set at 3 cm to maintain uniform flow distribution. A total of 27 pieces were used, distributed symmetrically and strategically to optimize the space and test conditions, as shown in Figure 3. The materials selected for the blocks were chosen for their durability and resistance to water, ensuring consistent performance throughout the experiments.

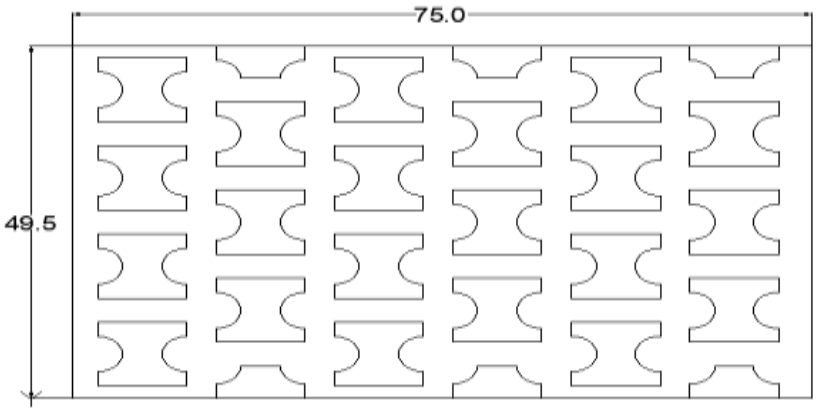

Fig. 3 Creating heat sinks in AutoCAD

In Autodesk Inventor, the Start 2D Sketch option was clicked, and the XY plane was chosen. Then, the complete design was imported and pasted into the Inventor window. After verifying that all measurements were correct, the design was centered precisely. The Patch option was selected to create a surface from the sketch, and consequently the file was saved.

In Autodesk CFD, water was selected as the working fluid due to its relevance for the hydraulic conditions under this investigation. The flow inlet velocities were set at 0.020 m/s and 0.029m/s for two different scenarios, with an inlet pressure of Pa and an outlet pressure condition set to 0.

For the Mesh Size option, an element size of 0.5 mm was selected to balance computational efficiency with the need for detailed and accurate results. The fine mesh allowed capturing intricate flow patterns, particularly around areas expected to have high gradients in velocity and pressure. A total of 1000 iterations were configured to ensure convergence, providing a balance between simulation time and result accuracy.

The SST Omega DES model was selected for the Turbulence option, as it offers a robust approach for capturing both laminar and turbulent flow characteristics, essential for accurately simulating complex flow behaviors in this study. The temperature option was disabled, as thermal effects were not within the scope of this analysis.

Finally, the Solve option was clicked to initiate the simulation process, allowing Autodesk CFD to conduct a numerical analysis based on the defined boundary conditions and flow models. This step enabled detailed insights into the flow dynamics, validating the design's performance under the specified conditions.

For a better view of the data required in this project, it can be viewed in the following figure 4 using this flow chart.

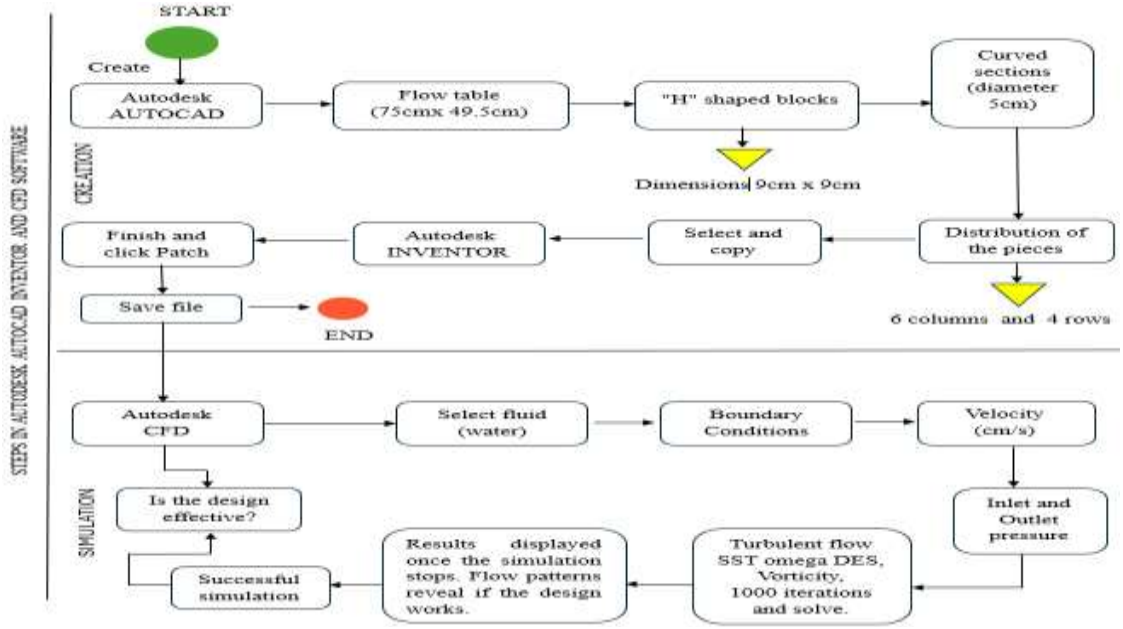

Fig. 4 Flowchart of steps in AutoCAD, Inventor and CFD software

Next, we will mention in detail the process of the experimental tests that were carried out with the H-shaped blocks: Before starting the test, the surface of the laminar flow table was cleaned to remove impurities that could cause friction in the water and to specify the results. Subsequently, the frosted glass was removed to facilitate the development of the experiment.
Then, the surface of the laminar flow table was cleaned to remove impurities that could cause friction in the water. Once this was done, the ink was prepared to allow the flow patterns to be observed during the test. To do this, it was mixed homogeneously with the water. To carry out the simulation, the designed blocks were placed, which were made of cement and plaster, previously glued to the acrylic base following the measurements specified in the plan. Afterwards, the acrylic with the pieces was taken to the laboratory table to then glue the ends to prevent water from filtering.
Once the blocks were placed as shown in Figure 5, the water tap was partially opened, allowing the initial flow to be laminar. This adjustment is important to observe a controlled flow in the first phase of the simulation. We let the water flow through the table; at this point, we proceeded to take measures to determine the flow rate and temperature.

Fig. 5 Placing blocks on the test table.

The length of the flow surface and the average height of the water were measured with a ruler. The water temperature was recorded to determine its viscosity and density, essential for accurate flow analysis.
As the tank was filled, the water height was measured at 1 cm increments up to 10 cm, with the exact time recorded at each increment using a stopwatch. This allowed the calculation of the flow rate.
Finally, ink was added to visualize the water currents, and fluorescent light improved the clarity of flow patterns and vortex formation around the H-shaped energy dissipators, as shown in Figure 6.

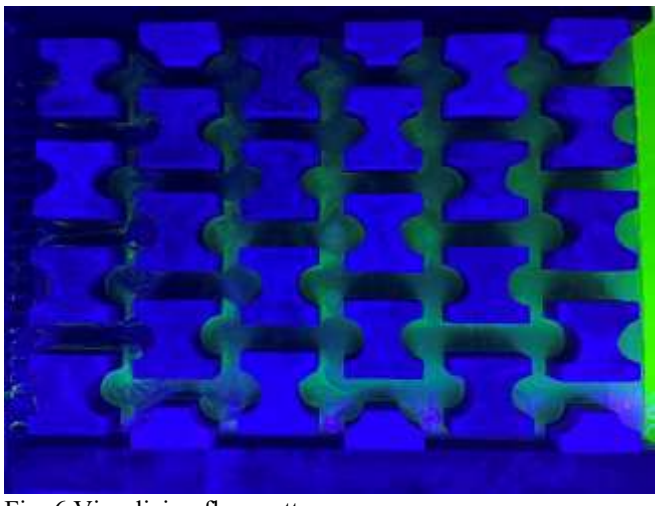

Fig. 6 Visualizing flow patterns

TPM Vol. 32, No. S6, 2025
ISSN: 1972-6325
https://www.tpmap.org/

Open Access

RESULTS

For this investigation, CFD simulations and experimental studies were compared to evaluate the kinematic behavior of water interacting with H-shaped energy dissipators. A temperature of 19.6 °C was used to determine the density and dynamic viscosity. Measurements of the flow table were conducted to calculate the hydraulic diameter, as shown in Table I, providing essential data for the analysis.

TABLE I DATA FOR DETERMINING THE REYNOLDS NUMBER

Temperature (°C)	Density (kg/m³)	Dynamic viscosity (Pa.s)	Hydraulic diameter (m)
19.6 °C	998.65	0.0010304	0.02

Likewise, the times had to be recorded for a height variation of 0.1 m, depending on the average times, an average speed could be calculated that helped us calculate the Reynolds number for both cases, explained in tables 2 and 4.

Tables 3 and 5 show the corresponding calculation to find the Reynolds numbers for both flow conditions.

TABLE II CALCULATION TO DETERMINE THE INLET VELOCITY FOR THE LAMINAR CASE

Climbing heights (m)	Average times (seg)	Δ Volume (m³)	Q Exit (m³/s)	Input speed (m/s)
0.01	20.42	0.00056	$2.73*10^{-5}$	0.011
0.02	8.85	0.00056	$6.31*10^{-5}$	0.025
0.03	9.14	0.00056	$6.10*10^{-5}$	0.025
0.04	9.66	0.00056	$5.78*10^{-5}$	0.023
0.05	11.35	0.00056	$4.92*10^{-5}$	0.020
0.06	12.69	0.00056	$4.40*10^{-5}$	0.018
0.07	12.36	0.00056	$4.51*10^{-5}$	0.020
0.08	11.38	0.00056	$4.90*10^{-5}$	0.020
0.09	10.83	0.00056	$5.15*10^{-5}$	0.021
0.1	10.67	0.00056	$5.25*10^{-5}$	0.021
	11.73			0.020

TABLE III DATA FOR CALCULATING REYNOLDS NUMBER FOR LAMINAR FLOW

Density (kg/m³)	Input speed (m/s)	Dynamic viscosity (Pa.s)	Hydraulic diameter (m)	Reynolds Number
998.65	0.020	0.0010304	0.02	384.23

TABLE IV CALCULATION TO DETERMINE THE INLET VELOCITY FOR TURBULENT CASES

Climbing heights (m)	Average times (seg)	Δ Volume (m³)	Q Exit (m³/s)	Average speed (m/s)
0.01	3.32	0.00056	$1.68*10^{-4}$	0.017
0.02	1.83	0.00056	$3.04*10^{-4}$	0.031
0.03	1.88	0.00056	$2.30*10^{-4}$	0.030
0.04	2.33	0.00056	$2.40*10^{-4}$	0.024
0.05	1.83	0.00056	$3.05*10^{-4}$	0.031
0.06	1.83	0.00056	$3.05*10^{-4}$	0.031
0.07	1.82	0.00056	$3.06*10^{-4}$	0.031
0.08	1.82	0.00056	$3.06*10^{-4}$	0.031
0.09	1.73	0.00056	$3.22*10^{-4}$	0.033
0.1	1.83	0.00056	$3.04*10^{-4}$	0.031
	2.02			0.029

TABLE V DATA FOR CALCULATING REYNOLDS NUMBER FOR TURBULENT FLOW

Density (kg/m³)	Input speed (m/s)	Dynamic viscosity (Pa.s)	Hydraulic diameter (m)	Reynolds Number
998.65	0.029	0.0010304	0.02	2071.23

For the CFD simulations, the flow was assumed to be incompressible, steady and ideal. This was assumed to simplify the complexity of the calculations. In turn, the flow effects allow the analysis to be focused in detail on the flow velocities and pressures throughout the circuit.

1) Results obtained for laminar conditions

In the laminar case, an inlet velocity of 0.0202 m/s was considered, with an inlet pressure of 30 Pa and an outlet pressure of 0 Pa. To determine the simulation solution, a parameter of 1000 iterations was set, despite this, results were obtained at 181 iterations.

Figure 7 shows sections of smaller area whose velocities range from 0.07 m/s to 0.11 m/s. This increase in velocities is due to the decrease in areas between dissipators, which forces the flow to increase its speed to maintain a constant flow throughout the circuit.

In addition, trace lines show the flow path in the channel in detail, facilitating thorough visual analysis. This approach allows for precise identification of velocity variations throughout the simulation, providing a better understanding of the flow behavior in each section of the circuit.

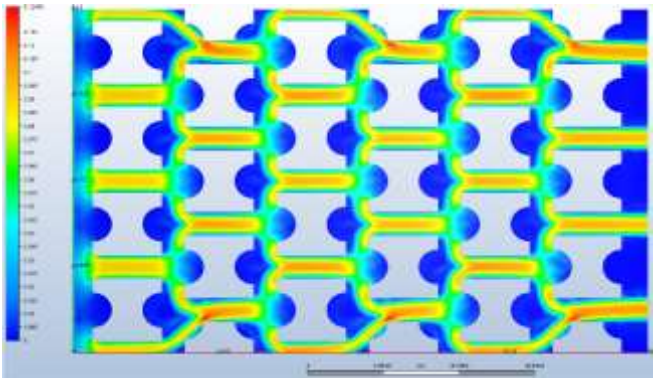

Fig. 7 Plan view with parameters of 0.020 m/s

In Figure 8, inlet pressures of 30.49 Pa and outlet pressures of -0.93 Pa are observed, showing a gradual decrease in pressure as the flow passes through the H-shaped dissipators. This decrease in pressure is mainly due to energy losses caused by friction. The pressures at the inlet are higher due to the initial impact between the flow and the dissipator, which causes a build-up of pressure before the water begins to move. Throughout the simulation, the pressure is considerably reduced to the point of presenting negative pressures, caused by the formation of small wakes and recirculation zones.

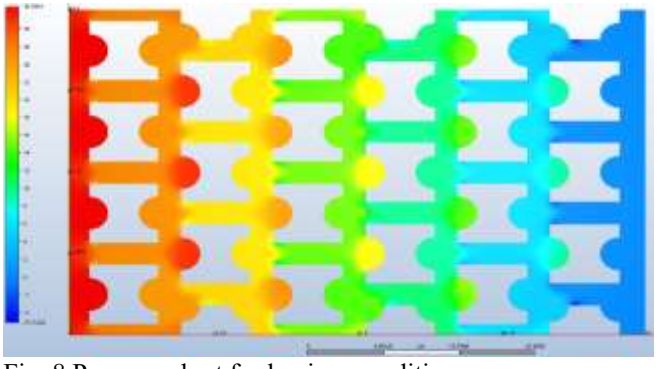

Fig. 8 Pressure chart for laminar conditions

For the experimental simulation represented in Figure 9, the water streamlines and their behavior when passing through smaller sections are observed. In these areas, there is an increase in speed due to the reduction of space, which affects the distribution of speeds throughout the circuit. In addition, stagnation points are identified, where the speed decreases to the point of reaching 0 m/s, guaranteeing the formation of eddies that help dissipate energy. For laminar flow, the streamlines can be visualized in detail and how the velocity vectors adapt to the geometry of the circuit.

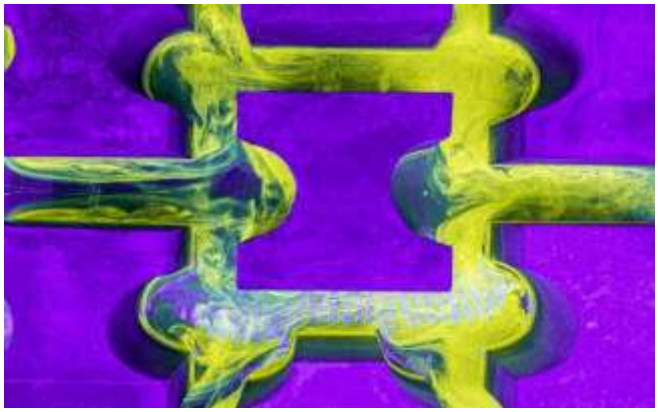

Fig. 9 Experimental simulation for laminar flow

Figure 10 shows in detail the behavior of the flow trace lines in front of an H-shaped energy dissipator. When interacting with the surface, it can be seen how the velocities decrease in a range of 0.034 m/s to 0.42 m/s due to the drag force, forming eddies in the semicircular part of the model. When compared with Figure 9, the kinematic similarity effect is evident, reflecting a similarity in the flow trajectory and how the same vorticity and wake are generated for both simulations.

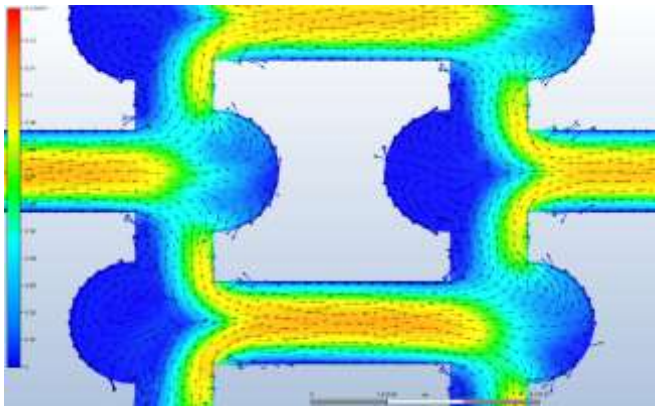

Fig. 10 CFD simulation with parameters 0.0202 m/s

2) Results obtained for turbulent conditions

For turbulent conditions, an inlet velocity of 0.0288 m/s, an inlet pressure of 30 Pa and an outlet pressure of 0 Pa were considered. Similarly, a parameter of 1000 iterations was established for the simulation, despite this, results were obtained at 328 iterations. The 10 corresponding simulations were carried out for the turbulent case and the SST K-Omega DES model was chosen due to its capacity to simulate with high precision the characteristics of the flow under turbulent conditions, especially in areas of high vorticity and flow separation effects. This model was chosen because it presented a high similarity with the results of the experimental test.

As can be seen in Figures 11, at the beginning of the flow an increase in speed is recorded and as the flow advances, the speed is progressively reduced, making it possible to see how the kinetic energy is dissipated. Likewise, the formation of wakes is observed in the circular areas of our design, which generates negative pressures in those areas. These effects demonstrate the effectiveness of the SST K- Omega DES model to accurately simulate turbulent phenomena and energy dissipation at high speeds.

Figure 11 shows in detail the behavior of turbulent flow and how the design dissipates kinetic energy through the eddies generated by the decrease in speed along its path. In areas of smaller areas, there is a maximum range of speeds between 0.08 m/s and 0.12 m/s. As the water passes through these areas and collides with the dissipators, a decrease in speeds between 0.02 m/s and 0 m/s occurs, due to the vorticity generated by the design. Furthermore, in these study areas, a pressure range between 0.05 Pa and 26.42 Pa is evident, due to stagnation effects expected in the hydraulic energy dissipation process as shown in Figure 12.

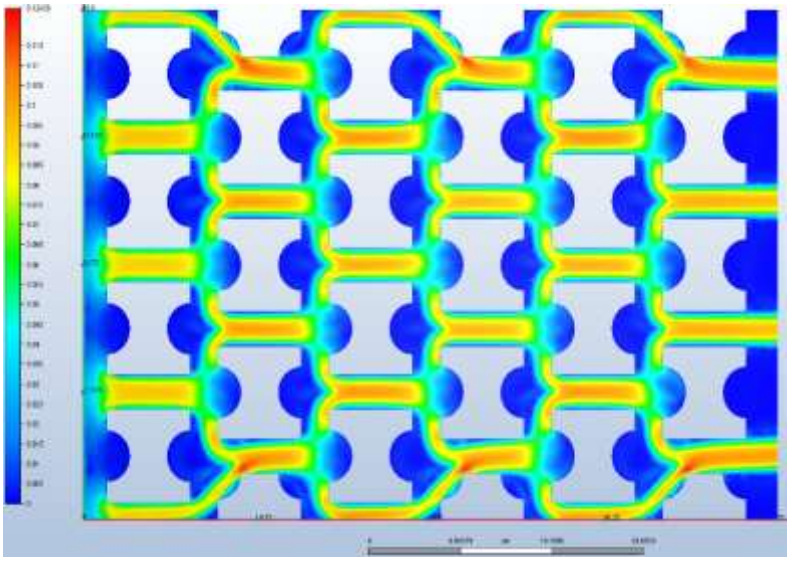

Fig. 11 Autodesk CFD simulation for turbulent flow

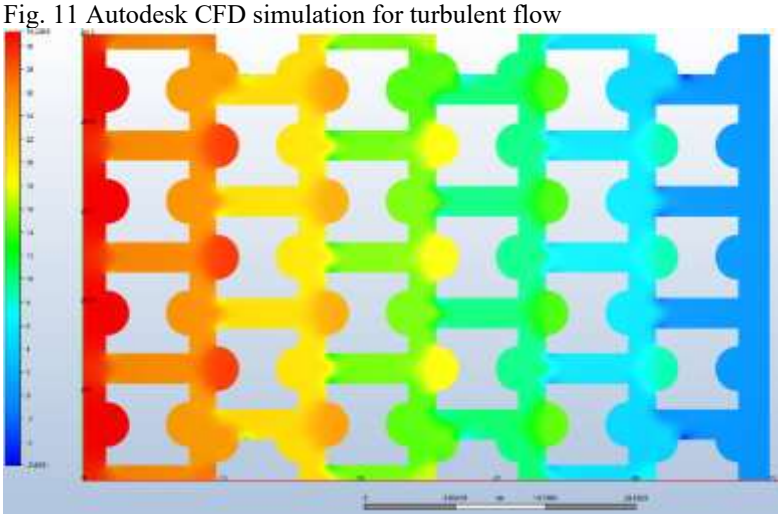

Fig. 12 Visualizing flow patterns

In Figure 13, it is clearly evident how the trace lines conform to the geometry of the design, which shows the flow detachment points in front of the H-shaped dissipator, where eddies are formed due to the presence of velocities close to 0 m/s. In addition, small Von Kárman effects can be seen caused by the oscillation of the vortices generated by the energy dissipator, a characteristic phenomenon of turbulent flow.

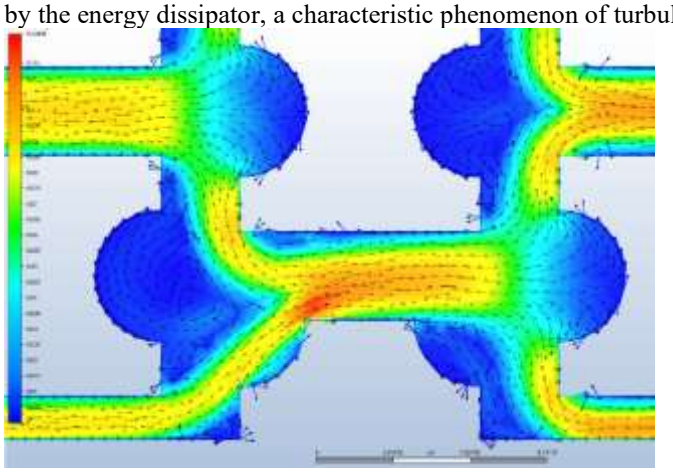

Fig. 13 Velocity vector visualization for turbulent flow

Similarly, in Figure 14 a progressive increase in speed is observed in this area where the area through which the fluid passes is reduced. This effect is produced to maintain the kinetic energy, which causes the flow to accelerate in order to maintain the flow rate in this area. At the stagnation points, present at the edges of the dissipator, is where drag forces are generated that reduce the speeds due to the resistance of the movement, which is essential for the dissipation of hydraulic energy. Likewise, a kinematic similarity was found with Figure 13, where the behavior of

the flow in front of the H-shaped energy dissipator is evident, evidencing similar patterns and effects such as the small wakes generated in this study area.

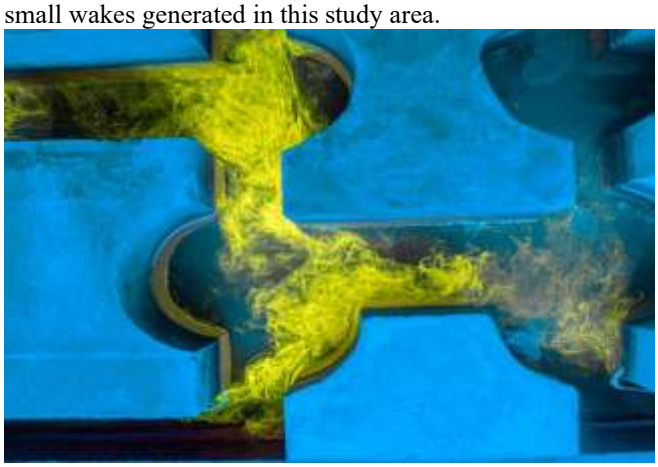

Fig. 13 Velocity vector visualization for turbulent flow

CONCLUSIONS

The results of this research have shown a remarkable similarity between the computational simulations carried out in Autodesk CFD and the experimental tests, confirming the accuracy of the model to predict the flow behavior under ideal conditions. The similarity between both methods is confirmed by observing consistent flow patterns, both in the behavior of the streamlines and in the distribution of velocities and pressures along the channel. In both cases, for both laminar and turbulent flow, similar trajectories and energy dissipation zones were shown, indicating that the computational model managed to capture the velocity and pressure changes characteristic of an energy dissipator.

Likewise, the design of the "H"-shaped energy dissipator generated eddies in strategic areas, which played a fundamental role in reducing the flow velocity at specific points in the channel. These eddies, generated both in the experimental and computational models, revealed the ability of the design to induce flow patterns that promote greater energy dissipation. This contributed significantly to the research that seeks to minimize the impact of the flow against exposed structures in civil works such as the construction of canals. In these areas, it is seen how the velocities are reduced to the point of reaching 0 m/s, minimizing the risk of erosion of the structures.

The presence of Von Kármán vortices in turbulent conditions was particularly relevant, since these recirculation phenomena contribute to the progressive reduction of the flow energy, minimizing the impact of the flow. The coherence observed in the formation of these eddies and vortices between the simulations and the experimental tests reinforces the validity of the computational model to represent complex flow dynamics.

In conclusion, the 'H'-shaped energy dissipator design demonstrated its effectiveness in achieving the objectives of this research by efficiently dissipating energy. The model's ability to reduce flow velocity at critical points through the generation of strategic eddies and Von Kármán vortices underscores its potential to protect structures from erosion. Furthermore, this research presents an innovative and practical solution for hydraulic engineering, offering a novel approach to energy dissipation and erosion control.

REFERENCES

[1] M. S. Alejos López, C. L. Trujillo Torres, and A. Carmona Arteaga, «Design study for hydraulic energy dissipator in streams using Autodesk CFD,» Lima, Perú, 2024. [En línea]. Disponible en: http://dx.doi.org/10.18687/LACCEI2024.1.1.176

[2] J. I. Janampa Guardia, H. J. Jacinto Ferrer, y A. Carmona Arteaga, «Study of semicircular sections through CFD software for rainwater retention in arid areas,» Lima, Perú, 2024. [En línea]. Disponible en: http://dx.doi.org/10.18687/LACCEI2024.1.1.175

[3] Software Autodesk Inventor | Obtener precios y comprar el producto oficial Inventor 2025. (s. f.). [En línea]. Disponible en: https://www.autodesk.com/es/products/inventor/overview?term=1-YEAR&tab=subscription&plc=INVPROSA

[4] A. Carmona Arteaga, G. A. Trigueros Cervantes, y N. Campos Vasquez, «Computational Fluid Dynamics (CFD) modeling of the local scour effect on circular bridge piers, » Lima, Perú, 2022. [En línea]. Disponible en: http://dx.doi.org/10.18687/LEIRD2022.1.1.202

[5] U. R. Mott and J., Mecanica de fluidos (7ma ed), addison Wesley, 2015, pp. 181 - 182.

[6] C. D. Castrillón Rosero y W. A. Tipán Tipán, «Análisis CFD del porcentaje de disipación de energía en rápidas escalonadas con flujo rasante para caudales pluviales de las zonas norte, centro y sur de la cuidad de Quito,» 2023. [En línea]. Disponible en: https://dspace.ups.edu.ec/handle/123456789/24261

[7] J. M. C. Yonus A. Cengel, Mecanica de fluidos Fundamentos y aplicaciones, Mc Graw Hill, 2015, pp. 11-133-340-586-593.

[8] I. González Neria, «Análisis de patrones turbulentos de un tanque agitado, utilizando dinámica de fluidos computacional y velocimetría por imágenes de partículas, » 2021. [En línea]. Disponible en: http://dx.doi.org/10.24275/uama.6747.8477
[9] O. A. Morales Contreras, J. A. Paz González, E. Hernández Martínez, M. Cortes Rodríguez, y G. Luna Serrano, «Coeficiente de arrastre de modelos circulares y cuadrados instalados en túnel de viento de ECITEC,» 2018. [En línea]. Disponible en: https://dialnet.unirioja.es/servlet/articulo?codigo=7989832
[10] B. R. Munson, Fundamentos de mecánica de fluidos, (7ma ed), Wiley, 2013, p. 127
[11] E. M. L. V. B. B. L. P. L. D. Landau, Mecanica de Fluidos volumen 6, Madrid: Reverté, S. A., 2021, p. 24.
[12] E. Amalia, M. A. Moelyadi, y M. Ihsan, «Efectos del modelo de turbulencia y pasos de tiempo numérico en el comportamiento del flujo de von Karman y la precision de arrastre de un cilindro circular, » 2018. Doi: 10.1088/1742-6596/1005/1/012012
[13] E. Morente Amado, «Estudio del efecto del borde de salida en el desprendimiento de vórtices generado por una cascada de álabes. »2019. [En línea]. Disponible en: http://hdl.handle.net/2117/173669
[14] L. D. Mendoza and L. E. V. Duarte, «Estudio de diferentes modelos de turbulencia para obtener las curvas características de un perfil naca 2415 mediante la simulación tridimensional de flujos de fluidos, » Colombia, 2019. [En línea]. Disponible en: http://repositorio.ufps.edu.co/handle/ufps/333
[15] F. M. White, Fluid Mechanics, 7th ed. New York: McGraw-Hill, 2016, p. 37.
[16] L. M. Álvarez Vitola y R. A. Briceño Miranda, «Diseño y elaboración de un sistema de tuberías para el análisis de la ecuación general de la energía,» Universidad de La Costa, 2021. [En línea]. Disponible en: https://hdl.handle.net/11323/8945
[17] O. Ortiz Vera, «Similitud hidráulica de sistemas hidrológicos altoandinos y transferencia de información hidrometeorológica, » tesis doctoral, Doctorado en Recursos Hídricos, Escuela de Posgrado, Universidad Nacional Agraria, La Molina, 2016. [En línea]. Disponible en: https://www.redalyc.org/articulo.oa?id=353543299002
[18] R. F. Estrada, «Análisis numérico de la estructura del flujo turbulento inerte en la estela cercana de un quemador tipo bluff-body circular usando herramientas computacionales de código abierto,» 2024. [En línea]. Disponible en: http://hdl.handle.net/20.500.12404/23888